Journal of Loss Prevention in the Process Industries 61 (2019) 220–236

Contents lists available at ScienceDirect

Journal of Loss Prevention in the Process Industries

journal homepage: www.elsevier.com/locate/jlp

Blind-prediction: Estimating the consequences of vented hydrogen deflagrations for inhomogeneous mixtures in 20-foot ISO containers

Trygve Skjold[a,b,*], Helene Hisken[a], Laurence Bernard[a], Lorenzo Mauri[a], Gordon Atanga[a], Sunil Lakshmipathy[a], Melodia Lucas[a], Marco Carcassi[c], Martino Schiavetti[c], Vendra Chandra Madhav Rao[d], Anubhav Sinha[d], Jennifer X. Wen[d], Ilias C. Tolias[e], Stella G. Giannissi[e], Alexandros G. Venetsanos[e], James R. Stewart[f], Olav Roald Hansen[g], Chenthil Kumar[h], Laurent Krumenacker[i], Florian Laviron[j], Romain Jambut[j], Asmund Huser[k]

[a] Gexcon, Fantoftvegen 38, 5072 Bergen, Norway
[b] University of Bergen, Allégaten 55, 5007 Bergen, Norway
[c] University of Pisa, Largo Lucio Lazzarino 2, 56122 Pisa, Italy
[d] Warwick FIRE, School of Engineering, University of Warwick, Coventry, UK
[e] Environmental Research Laboratory, National Center for Scientific, Research Demokritos, Agia Paraskevi, 15310, Greece
[f] HSE, Harpur Hill, Buxton, Derbyshire, SK17 9JN, UK
[g] Lloyd's Register, Kokstadflaten 35, 5863 Bergen, Norway
[h] Fluidyn, 146 Ring Road, Bangalore, 560102, India
[i] Fluidyn, 7 Blvd. de la Libération, 93200 Saint-Denis, France
[j] DNV GL, 69 Rue Chevaleret, 75013 Paris, France
[k] DNV GL, Veritasveien 1, 1337 Høvik, Norway

ARTICLE INFO

Keywords:
Blind-prediction
Vented deflagration
Hydrogen safety
Inhomogeneous mixtures

ABSTRACT

This paper summarises the results from a blind-prediction benchmark study for models used for estimating the consequences of vented hydrogen deflagrations, as well as for users of such models. The work was part of the HySEA project that received funding from the Fuel Cells and Hydrogen Joint Undertaking (FCH JU) under grant agreement no. 671461. The first blind-prediction benchmark exercise in the HySEA project focused on vented explosions with homogeneous hydrogen-air mixtures in 20-foot ISO containers. The scenarios selected for the second blind-prediction study focused on vented deflagrations in inhomogeneous hydrogen-air mixtures resulting from continuous stratification of hydrogen during vertical jet releases inside 20-foot ISO containers. The deflagrations were vented through commercial vent panels located on the roof of the containers.

The test program included two configurations and four experiments, i.e. two repeated tests for each scenario. The paper compares experimental results and model predictions and discusses the implications of the findings for safety related to hydrogen applications. Several modellers predicted the stratification of hydrogen inside the container during the release phase with reasonable accuracy. However, there is significant spread in the model predictions, especially for the maximum reduced explosion pressure, and including predictions from different modellers using the same model system. The results from the blind-prediction benchmark studies performed as part of the HySEA project constitute a strong incentive for developers of consequence models to improve their models, implement automated procedures for scenario definition and grid generation, and update training and guidelines for users of the models.

1. Introduction

This section describes the motivation and context for the blind-prediction benchmark study.

1.1. Vented hydrogen deflagrations

Several properties of hydrogen differ significantly from most conventional and alternative fuels (Astbury, 2008). The low boiling point of liquid hydrogen and the low density of gaseous hydrogen, relative to

* Corresponding author. University of Bergen, Department of Physics and Technology, Allégaten 55, 5007, Bergen, Norway.
E-mail address: trygve.skjold@uib.no (T. Skjold).

https://doi.org/10.1016/j.jlp.2019.06.013
Received 23 March 2019; Received in revised form 13 June 2019; Accepted 14 June 2019
Available online 18 June 2019

air, implies that loss of containment in confined spaces is likely to result in stratified mixtures (Gallego et al., 2007; Makarov et al., 2018). Furthermore, due to the low ignition energy and wide flammability range of hydrogen-air mixtures (Ono et al., 2007), fires and explosions represent a significant hazard for most hydrogen installations.

Hydrogen deflagrations in stratified mixtures are inherently complex phenomena. The laminar burning velocity of hydrogen-air mixtures is significantly higher than for most conventional and alternative fuels (Konnov et al., 2018), and various hydrodynamic, thermo-diffusive and thermo-acoustic instabilities may influence the flame (Clavin and Searby, 2016). The role of thermo-diffusive instabilities will depend on the mixture composition (Sánchez and Williams, 2014): cellular instabilities occur at sufficiently fuel-lean conditions (negative Markstein lengths), and pulsating instabilities occur at sufficiently fuel-rich conditions (positive Markstein lengths).

Most accidental gas explosions in industry entail transient turbulent flame propagation in geometries with various degree of congestion and confinement. Of particular concern for hydrogen-air mixtures is the propensity to undergo deflagration-to-detonation-transition (DDT) under certain conditions (Ciccarelli and Dorofeev, 2008). To this end, specific measures are generally required for reducing the explosion risk in hydrogen systems to a tolerable level (Dorofeev et al., 1994; Crowl and Jo, 2007; Rigas and Amyotte, 2013; Fuster et al., 2017; Skjold et al., 2017, 2018; Moradi and Groth, 2019).

Explosion mitigation by venting is frequently used for reducing the consequences of hydrogen deflagrations in confined systems (Bauwens et al., 2011, 2012; Bauwens and Dorofeev, 2014; Skjold et al., 2019b). However, it is not straightforward to design optimal systems for explosion protection. By varying parameters such as leak location, leak direction, leak rate, leak profile/duration, natural ventilation, forced ventilation and ignition position, numerous accident scenarios can be realised for a given installation. Furthermore, the phenomena involved are inherently complex, including the turbulent combustion and the two-way interaction between the transient pressure load from the explosion and the structural response of the enclosure and the venting device. The limited repeatability of large-scale deflagration experiments in congested geometries suggests that the chain of events is highly sensitive to the initial and boundary conditions (Evans et al., 1999; Skjold, 2018b; Skjold et al., 2019a).

Models for estimating the consequences of vented hydrogen deflagrations range from empirical or semi-empirical correlations (Razus and Krause, 2001; Sustek and Janovsky, 2013), to advanced model systems based on computational fluid dynamics (CFD) and finite element (FE) methods. Of particular concern from a modelling point of view, and especially for engineering calculations performed as part of risk assessments, are the inherent limitations concerning the spatial and temporal scales that can be resolved. Model developers must inevitably strike a balance between the accuracy and predictive capabilities of the model, calculation time, and the efforts required by users of the models to generate reliable results. Another relevant consideration is the level of conservatism incorporated in the model, given the inherent uncertainty and variability in experimental data for model validation. To this end, it is essential to validate and document the performance of consequence models for vented hydrogen deflagrations against large-scale experiments (Skjold et al., 2013).

1.2. Previous work

Vented hydrogen deflagrations have been extensively studied in the past, but primarily for initially quiescent mixtures ignited to deflagration in empty enclosures (Razus and Krause, 2001; Bauwens et al., 2011, 2012; Sustek and Janovsky, 2013; Bauwens and Dorofeev, 2014; Molkov and Bragin, 2015). Sommersel et al. (2008, 2017) investigated the effect of initial turbulence and congestion for vented hydrogen explosions in a 20-foot ISO container. Hooker et al. (2017) described an experimental program with vented deflagrations in a 31 m^3 low strength enclosure, conducted as part of the HyIndoor project.

Several blind-prediction benchmark studies have been conducted for hydrogen in the past (Gallego et al., 2007; García et al., 2010; Makarov et al., 2009; Baraldi et al. 2010, 2017; Skjold et al., 2019a). Baraldi et al. (2010) highlighted the need for blind-prediction benchmark studies for proper evaluation of the predictive capabilities of consequence models.

1.3. The HySEA project

The primary objective of the project *Improving Hydrogen Safety for Energy Applications through pre-normative research on vented deflagrations* (HySEA) was to develop recommendations for improved international standards for the design of explosion venting protective systems, such as EN 14994 (2007) and NFPA 68 (2018). The members of the HySEA consortium were Gexcon (coordinator), University of Warwick (UWAR), University of Pisa (UNIPI), Fike Europe, Impetus Afea and Hefei University of Technology (HFUT). The HySEA project included two blind-prediction benchmark studies where modellers were invited to submit model prediction for well-defined vented deflagration scenarios before the completion of the actual experiments. The results from the first study (Skjold et al., 2019a), which focused on vented deflagrations in homogeneous lean hydrogen-air mixtures, revealed significant spread in the model predictions, for CFD codes as well as simpler models based on empirical or semi-empirical correlations. This paper presents the results from the second blind-prediction benchmark study in the HySEA project.

1.4. The second HySEA blind-prediction benchmark study

The experimental program in the HySEA project included 66 vented hydrogen deflagration experiments performed in 20-foot shipping containers: 42 tests with initially homogeneous and quiescent mixtures, and 24 tests with inhomogeneous mixtures (Skjold, 2018a,b; Skjold et al., 2019b). The total number of tests was 72, which included five unignited dispersion tests and one failed test. The scenarios selected for the second HySEA blind-prediction benchmark exercise involved continuous stratification of hydrogen and subsequent ignition to deflagration and explosion venting through commercial vent panels.

The members of the HySEA consortium invited researchers and engineers to submit model predictions before the actual experiments were performed. The call for model predictions was published on the HySEA website and distributed by e-mail. The University of Pisa collected the model predictions submitted within the deadline on 30 November 2017. Three commissioning tests without ignition were completed in October 2017 (Table 1), but the results were not communicated to the modellers. Seven individuals/groups submitted predictions obtained with CFD tools, and one group submitted predictions from various models based on empirical or semi-empirical correlations.

Table 1
Test matrix for the second HySEA blind-prediction benchmark exercise, including commissioning tests and reference tests with homogeneous mixtures.

Test	Date	A_v (m^2)	Ign.	C_n (vol.%)	Geo.	T_{amb} (°C)
T39	19.10.2017	–	–	21 (nominal)	P2	9 ± 2
T42	23.10.2017	–	–	21 (nominal)	FO	12 ± 2
T43	23.10.2017	–	–	21 (nominal)	FO	14 ± 2
T46	30.10.2017	6.0	BU	21 (homog.)	FO	6 ± 2
T47	17.11.2017	6.0	BU	21 (homog.)	FO	6 ± 2
T48	17.11.2017	6.0	BU	21 (homog.)	P2	7 ± 2
T57*	30.11.2017	6.0	BU	21 (nominal)	FO	-3 ± 2
T59	05.01.2018	6.0	BU	21 (nominal)	FO	-3 ± 2
T60*	08.01.2018	6.0	BU	21 (nominal)	P2	3 ± 2
T61*	09.01.2018	6.0	BU	21 (nominal)	P2	0 ± 2

Fig. 1. 20-foot ISO container (left) and the interior of the container (right).

2. Experiments

This section describes the test rig, measurement system and experimental procedure, as described in the call for model predictions for the blind-prediction benchmark study.

2.1. Test rig

Gexcon performed the experiments in 20-foot containers at the remote test site on the island of Sotra outside Bergen. The experimental rig used for the HySEA experiments consisted of a standard 20-foot ISO container fitted with a steel frame on the floor. The purpose of the steel frame was to support obstacles and instrumentation inside the container and to fix the container to a solid foundation. Fig. 1 shows one of the twelve containers used in the experimental campaign (left) and the interior of a container ready for testing (right). The red arrow indicates the position and direction of the jet release. Fig. 2 shows the steel frame (the white structure on the floor in Fig. 1) placed on top of the foundation during the construction of the test rig.

Fig. 3 shows the overall dimensions of the steel frame and the position of the eight bolts used for fixing the frame and container to the foundation. The foundation was made from two 360-mm H-beams, which implies that the bottom of the container was positioned 0.36 m above ground level during testing. The steel frame was constructed from U-beams (UNP 200, Fig. 3). The U-beams positioned along the back wall and along both side-walls of the container had the flat side facing the container walls to minimise flame acceleration in the gap between the frame and the corrugated wall.

Fig. 4 summarises the overall dimensions of the containers. The inner dimensions were 5.87 m × 2.35 m × 2.39 m, for a total volume of about 33 m^2. The floor inside the containers was covered with plywood, and the walls and the roof were made of corrugated steel plates. The level of the floor was about 0.50 m above ground level during testing.

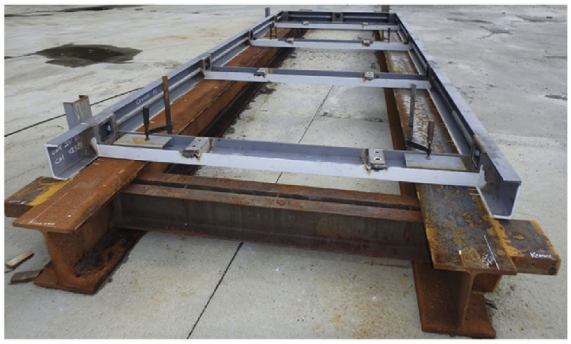

Fig. 2. The steel frame (grey) on top of the foundation.

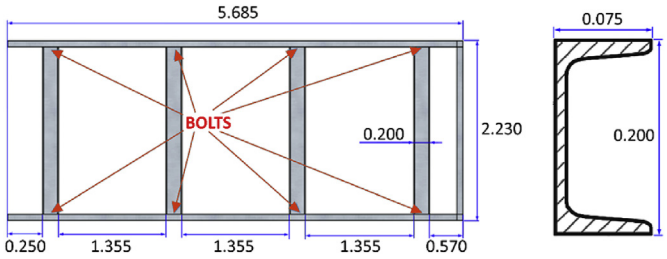

Fig. 3. Dimensions of the steel frame (left) and a cross-section of the U-beam (right).

The depth of the corrugations in the walls was 35 mm, one 'period' of corrugation 280 mm, and the plate thickness 2.0 mm.

The corrugated plate on the roof of the containers was replaced with a tailor-made steel frame that supported the vent panels. This frame was made from 100 mm × 100 mm square pipes and a 100 mm × 80 mm rectangular pipe along the centre. Eight chains tightened with turnbuckles connected the frame on the roof to the frame on the floor inside the container (Fig. 1). Six of the eight 1.0 m × 1.0 m openings were covered with single-sheet bulged vent panels with vent area A_v 1.0 m^2 and nominal static opening pressure P_{stat} 100 mbar. The remaining openings in the roof were closed with blind flanges. Fig. 5 illustrates the position of the vent panels, ignition source, pipe rack and jet release. The dimensions of the two blocked openings towards the container doors were 1.0 m × 0.56 m. Fig. 6 shows a container with six panels (A_v = 6.0 m^2) before and after a test (container doors on the left).

Fig. 7 shows the pipe rack obstacle. The obstacle consisted of a steel frame made from 100 mm × 100 mm square pipes. This frame supported four layers of round pipes: two shelves with five pipes each, pipe diameter 104 mm, 200 mm spacing, and fixed with U-bolts, and two shelves with 22 pipes in two layers, pipe diameter 20 mm, 100 mm spacing in horizontal direction, 33 mm spacing in vertical direction, and fixed with standard support clamps for hydraulic pipes. All pipes were 1200 mm long. The shelves for fixing the pipes were made from 50 mm × 50 mm angle steel, with heights above the floor of the container of 600, 800, 1100 and 1400 mm. The pipe rack was fixed with brackets to the frame inside the container. Fig. 1 (right) shows the pipe rack mounted in the centre position, denoted configuration P2. Three one-inch pipes (outer diameter about 34 mm) prevented the upper part of the container from bulging out. The centre of these pipes was about 80 mm below the frame that supported the vent panels.

2.2. Measurement system

Fig. 8 summarises the measurement system. Four NI CompactDAQ

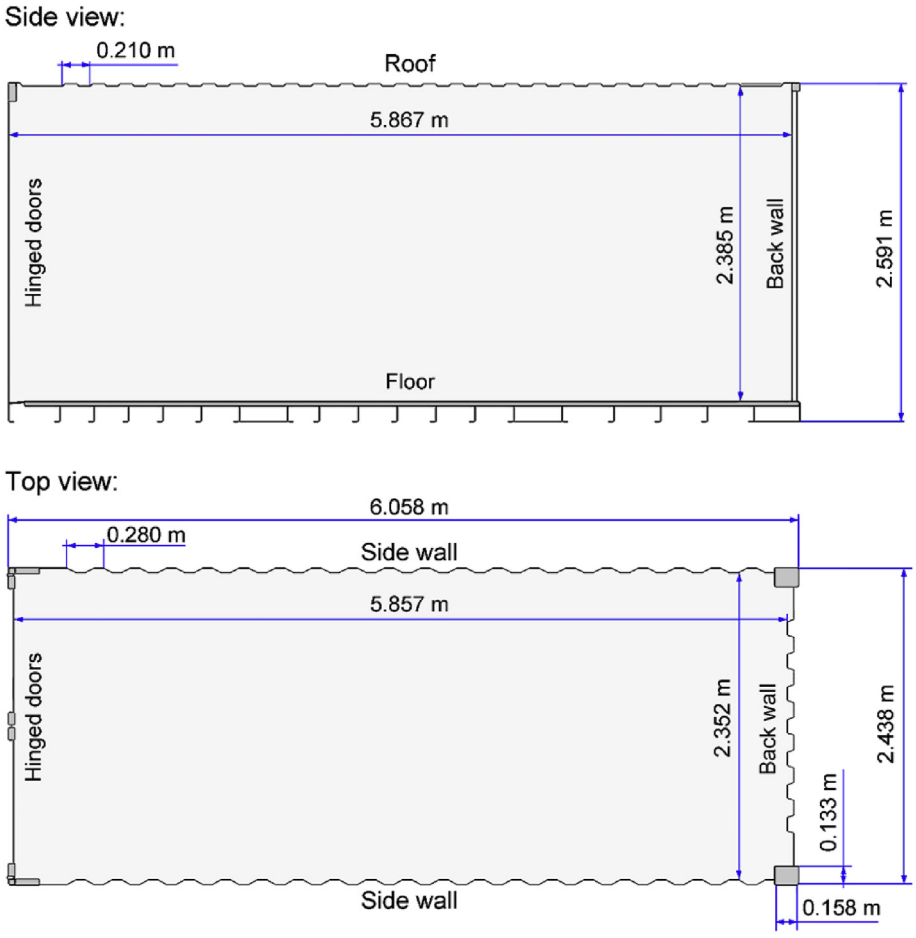

Fig. 4. Overall dimensions of a 20-foot ISO container.

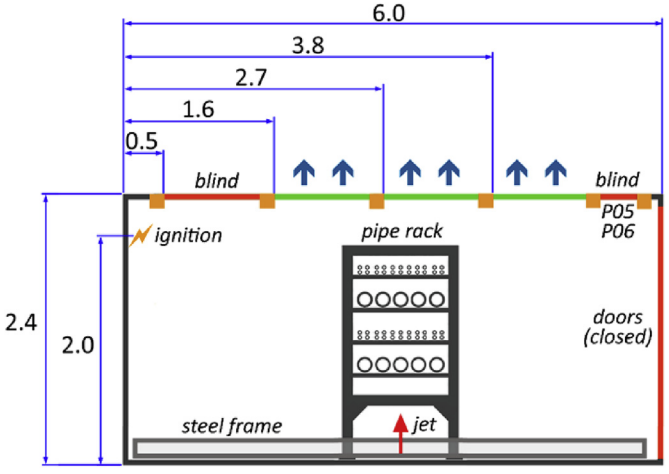

Fig. 5. Schematic illustration of container and vent openings.

Fig. 6. Container with six commercial vent panels before and after a test.

type 9215 (BNC) data acquisition modules from National Instruments, mounted in a cDAQ-9188XT chassis located in the instrumentation bunker, recorded the pressure and deflection measurements at a sampling frequency of 100 kHz. A separate National Instruments NI-9201 data logger was used for the concentration measurements. Two Edgertronic SC1 high-speed video cameras and one regular JVC GZ-RX515BE video camera recorded the explosion events.

Fig. 9 illustrates the position of the vertical jet release (R01) and the eight internal pressure sensors: P01-P04 (Kistler 701A, high-pressure quartz transducers), P05-P06 (Kistler 7261, low-pressure quartz transducers, high-sensitivity) and P07-P08 (Kistler 7031, high-pressure quartz transducers, acceleration-compensated), all used with Kistler 5073A charge amplifiers. The sensors P01-P02 and P07-P08 were positioned on the horizontal surface of the U-beams along the side walls of the container, in the same distances from the back wall as the bolts holding the frame (Fig. 3), 85 mm from the side wall, and 200 mm above the floor of the container. Sensors P03 and P04 were positioned at the vertical surface facing the container doors, about 100 mm above

Fig. 7. Pipe rack (left) and brackets fixed to frame inside the container (right).

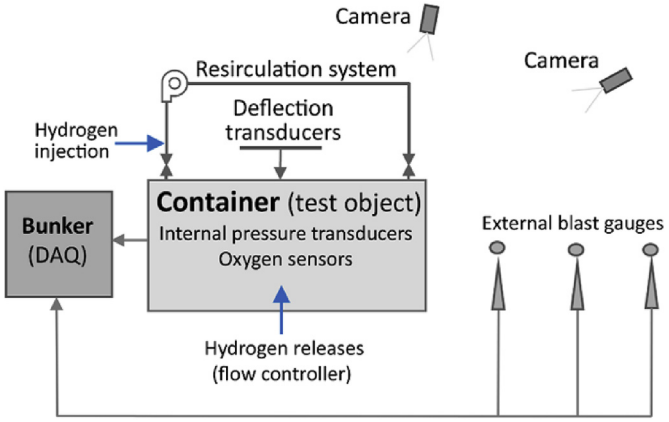

Fig. 8. Schematic overview of the measurement system.

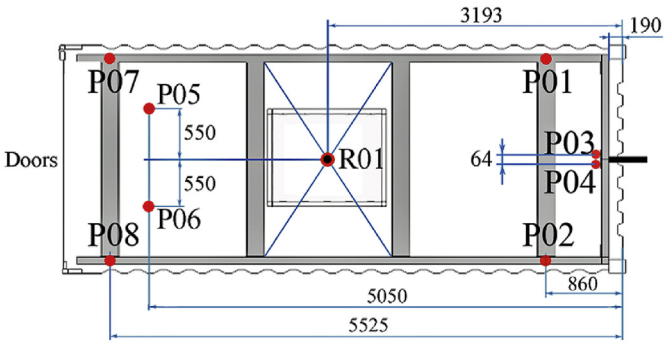

Fig. 9. Approximate positions (mm) for the internal pressure sensors P01-P08.

the floor level. The two low-pressure sensors P05 and P06 were positioned in the blind flanges in the ceiling, between the vent panels and the doors (Fig. 5). These measurements provide an estimate of the opening pressure of the vent panels. Due to the symmetry of the geometry, each pair of pressure sensors (P01 & P02, P03 & P04, etc.) should measure similar values.

Three Kistler 4043A2 piezoresistive absolute pressure gauges with Kistler 4601 amplifiers measured the far-field blast pressures P09-P11 outside the container, 5, 10 and 15 m from the container doors, and about 1.65 m above the ground. Two Acuity AR700-50 Laser displacement sensors, operating at 9.4 kHz, measured the structural displacement of the container walls. A digital thermal mass flow meter and controller from Brooks Instrument (Model SLA5853-S2EAB2C2A1) controlled the flow rate of hydrogen into the container. Fig. 10 illustrates the position of the concentration measurements in a vertical cross-section of the container.

Fig. 11 shows the front side of the container with the five sampling tubes for the Servomex Xendos 2223 oxygen transmitter/analyser in positions A4′-E4′, and the opposite side of the container with the eight low-cost oxygen sensors from Teledyne instruments (oxygen sensor class R-22A) in positions A1-E4. All measurements were taken close to the side walls. The symmetric location of the vertical row of probes (A4, B4, etc.) and sampling tubes (A4′, B4′, etc.) near the back wall implies that the continuous and intermittent concentration measurements should measure similar concentration profiles for the stratified mixture inside the container.

Fig. 12 shows the pipe used for the vertical jet release. The pipe had outer and inner diameters 22 mm and 18 mm, respectively. The release point was positioned along the centre line of the container, about 3.2 m from the back wall, 0.30 m above the floor, pointing upwards. A flat plate, with dimensions 0.2 m × 0.2 m, was located about 0.2 m below the release point. This plate was used for tests with diffusive releases (not part of the blind-prediction study). Measurements with thermocouples located in the jet, immediately downstream of the release point, indicated that the release temperature was within 1–3 °C of the ambient temperature.

Fig. 8 illustrates the recirculation system that consisted of 4-inch flexible air ducts, a fan, and two remotely operated butterfly valves (Fig. 11) for isolating the ducts and fan from the container prior to ignition. This system was not used for the tests with inhomogeneous mixtures, but it was installed as a precautionary measure in the event it would be necessary to empty flammable mixture from a container after failed ignition.

2.3. Experimental procedure

Gaseous hydrogen was released into the container at a constant flow rate of 56 $Nm^3\ hr^{-1}$ (equivalent to 0.00133 $kg\ s^{-1}$) through a vertical pipe with inner diameter 18 mm. The open end of the pipe was located 0.3 m above the floor of the container. The duration of the release was 7.5 min (450 s). Distributed openings in the side walls allowed excess gas to escape: 20 holes, ten on each side of the container, 51 mm (2 inches) in diameter, 100 mm above the floor (Fig. 11). The target nominal (average) fuel concentration C_n at the time of ignition, assuming only air escaped from the container, was 21.0 ± 0.5 vol% (Table 1). However, some fuel may have escaped, either through small openings in the ceiling or through the openings in the side walls close to the floor.

Hydrogen concentrations were measured near the corners of the container, in the opposite end from the container doors (Fig. 10 and 11), during the release and up to the time of ignition. The ignition source, an inductive spark with energy release about 1 mJ, was activated about 8 min (480 s) after the release started (i.e. 30 s after the release ended). The spark gap was located at the back wall, about 2.0 m above the floor (denoted BU in Table 1). The explosions were vented through six 1.0 m × 1.0 m vent openings on the roof of the container (Fig. 5), covered with single-sheet bulged vent panels from Fike: A_v = 1.0 m^2, P_{stat} = 0.10 ± 0.25 bar, and specific weight 6.8 $kg\ m^{-2}$. The container doors were closed.

3. Experimental results

This section summarises the results of the experiments.

3.1. Test matrix

Table 1 summarises the test matrix, including the three commissioning tests without ignition (T39, T42 and T43) and three reference tests with homogeneous mixtures (T46-T48). Fig. 5 illustrates the location of the vent openings, the jet release, the pipe rack and the ignition source. Tests 57 and 59 were repeated tests with frame only (FO), i.e. without the pipe rack present. Tests 60 and 61 were repeated tests with the pipe rack in the centre position (P2). Table 2 summarises

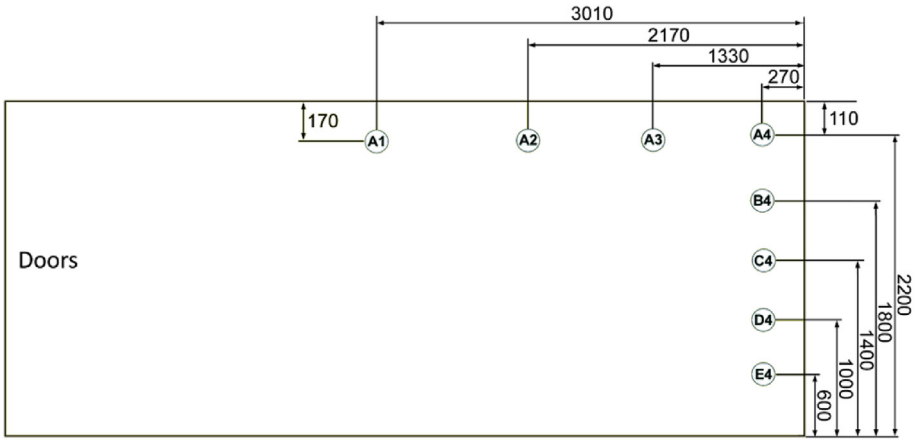

Fig. 10. Positions (mm) for the concentration measurements.

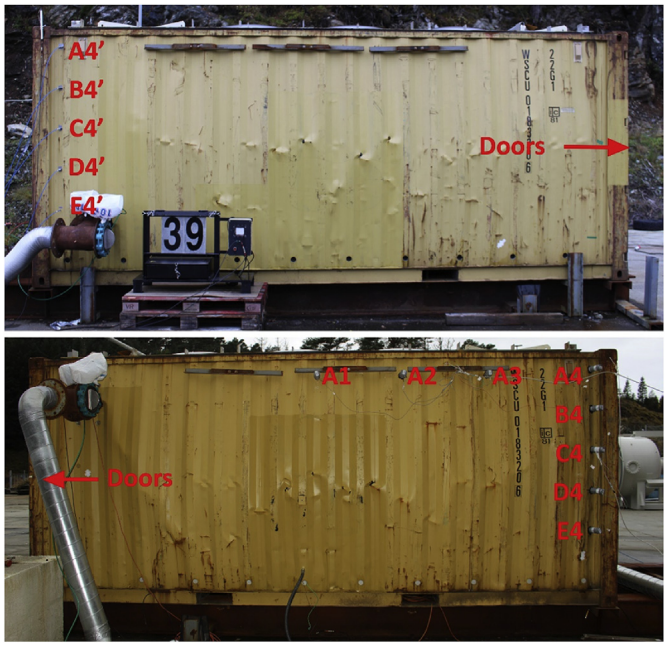

Fig. 11. The tubes for the Servomex analyser (above) and the low-cost oxygen sensors (below).

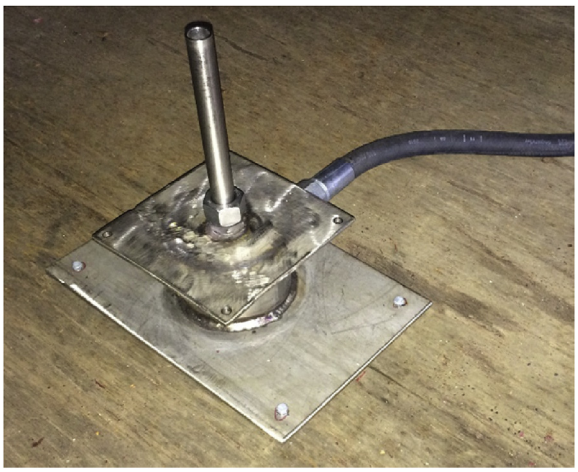

Fig. 12. Pipe used for vertical jet release.

selected results from the ignited tests: the maximum reduced explosion pressures P_{max} and the maximum pressure impulse I_m recorded by the internal pressure sensors P01-P08, the maximum deflection D_m and permanent deformation D_p measured with laser displacement sensors approximately 14 cm above the centre of the side walls (1.9 m above the ground), the time t_{stat} and internal pressure P_{stat} when the panels started to open, and the approximate times t_{45}, t_{90} and t_{180} relative to t_{stat} when the panels were 45°, 90° and 180° open, respectively. The asterisks for test numbers 57, 60 and 61 in Tables 1 and 2 indicate that the test container had to be replaced after these tests due to severe structural deformation.

3.2. Measurement uncertainties

The range of values given for the maximum reduced explosion pressures P_{max} in Table 2 illustrates the effect of applying digital smoothing filters, with frequencies 33, 50 and 100 Hz, to the measured pressure-time histories (Skjold, 2018a,b; Skjold et al., 2019b). The stated measurement error for the piezoelectric pressure sensors, typically less than ± 1% of full-scale output (FSO), is negligible compared to the inherent uncertainty associated with temperature drift, smoothing and spread in results between repeated tests. The parameters I_m, D_m and D_p were not sensitive to smoothing, and the laser-based displacement measurements (D_m and D_p) showed no sign of drift (Skjold, 2018a,b; Skjold et al., 2019b). The accuracy of the displacement measurements was within ± 0.002 m. The opening times for the vent panels were estimated from high-speed video recordings. Based on independent observation of recordings from two cameras in different locations, the accuracy of the time estimates was estimated to be within ± 0.002 s. The values indicated for P_{stat} are filtered pressure data (50 Hz) measured with the two sensors P05 and P06 at time t_{stat}. The measurement uncertainties of the concentration measurements were approximately ± 0.2 and ± 0.6 vol% for the point (Servomex) and continuous (Teledyne) measurements, respectively. The corresponding response times for the sensors (0–90 vol% O_2) were ten and six seconds.

3.3. Release rates

Fig. 13 summarises the flow rates measured with the digital thermal mass flow meter and controller. All measurements indicate a near constant flow rate of 56.0 ± 0.2 $Nm^3\,hr^{-1}$ for 450 s. However, it is not clear whether the deviation from zero (about 3 $Nm^3\,hr^{-1}$) in the initial flow for tests 57 and 59 imply that the actual flow rates for these tests were closer to 53 $Nm^3\,hr^{-1}$, especially since the curve for test 59 returns to zero while the curve for test 57 does not. The concentration profiles measured at 480 s (Fig. 17) show consistently lower concentrations for tests 57 and 59, relative to tests 42 and 43, indicating

Table 2
Selected results for ignited tests, including reference tests with homogeneous mixtures.

Test	P_{max} (bar)	I_m (bar-ms)	D_m (m)	D_p (m)	t_{stat} (s)	$P_{stat,\ P05\text{-}P06}$ (bar)	t_{45} (s)	t_{90} (s)	t_{180} (s)
57*	0.314–0.343	7.9	0.178	0.042	0.082	0.118–0.125	0.022	0.035	0.059
59	0.319–0.342	8.0	0.167	0.030	0.083	0.109–0.111	0.026	0.038	0.061
60*	0.344–0.370	9.6	0.185	0.064	0.096	0.108–0.115	0.025	0.036	0.058
61*	0.514–0.677	11.6	0.382	0.263	0.076	0.107–0.110	0.025	0.034	0.050
46	0.176–0.185	6.6	0.112	0.019	0.107	0.104–0.108	0.032	0.046	0.078
47	0.186–0.197	6.9	0.139	0.023	0.121	0.117–0.122	0.027	0.043	0.072
48	0.171–0.176	7.0	0.124	0.013	0.112	0.107–0.109	0.029	0.046	0.076

reduced flow rates and possible leakage. A constant flow rate at 53 Nm^3 hr^{-1} would correspond to a nominal (average) hydrogen concentration of about 20 vol% in the container.

3.4. Dispersion and stratification

Fig. 14 summarises the results from two unignited tests: T42 (FO) and T39 (P2). The vertical dash-dotted lines at 450 s indicate the end of the releases. There is reasonable agreement between the results obtained with the low-cost oxygen sensors from Teledyne (continuous

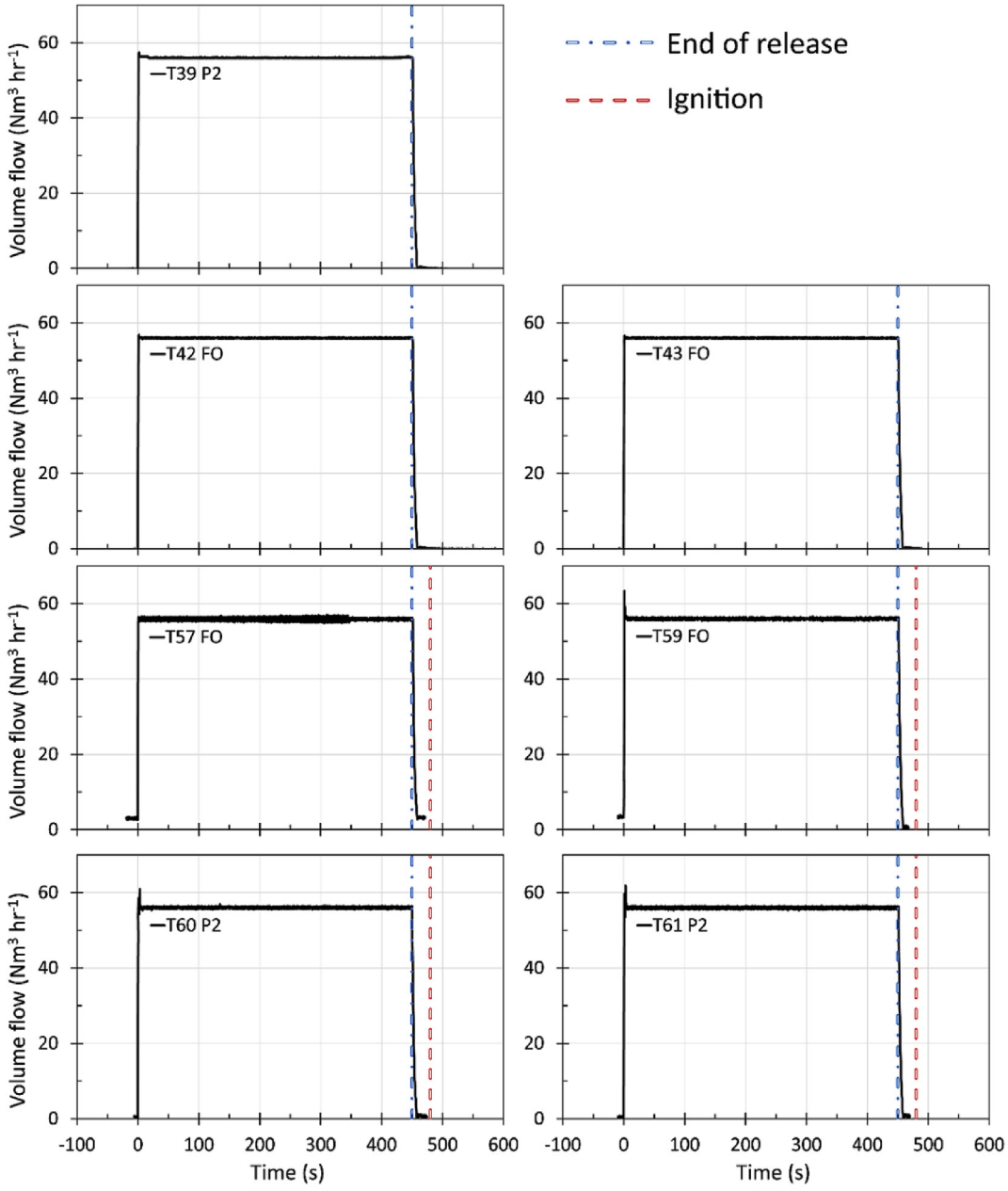

Fig. 13. Measured flow rates.

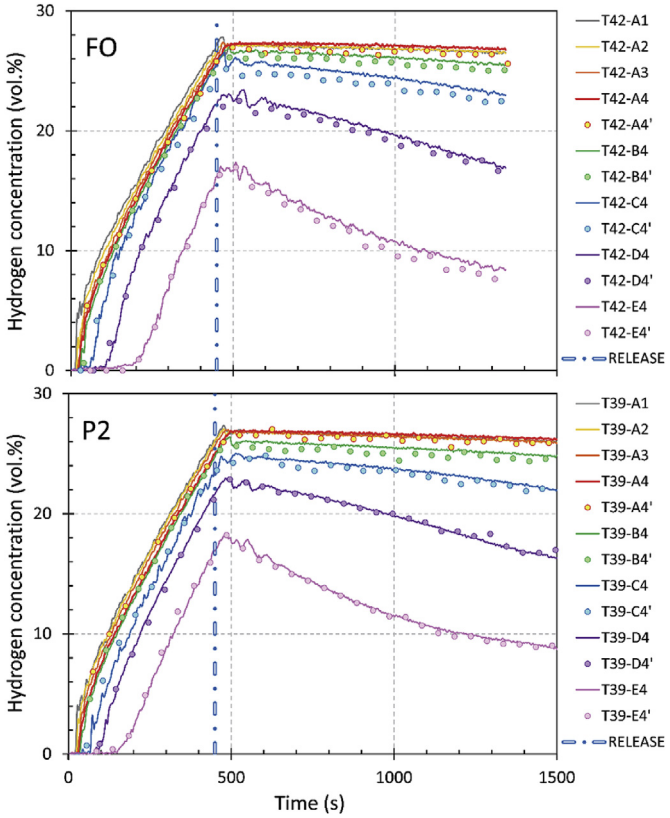

Fig. 14. Hydrogen concentrations for unignited tests with frame only (FO) and pipe rack (P2).

lines) and the intermittent measurements with the Servomex analyser (points). The results demonstrate clear stratification inside the container, with maximum hydrogen concentrations around 27 vol% near the ceiling. The pipe rack (P2) had limited influence on the distribution of hydrogen inside the enclosure.

Fig. 15 documents the repeatability of the dispersion process for ignited and unignited releases. The concentrations obtained for ignited tests 57, 59 and 60 are somewhat lower than the corresponding unignited tests 42 and 39. The results indicate that the flow rate may have been less than 56 $Nm^3\ hr^{-1}$ for tests 57 and 59 (Fig. 13) and that some fuel may have escaped through the roof. Since all measurements indicate mixtures on the lean side, i.e. below about 30 vol% hydrogen in air, a lower concentration at the time of ignition would result in lower maximum reduced explosion pressures in the vented deflagrations.

3.5. Pressure development

Fig. 16 shows smoothed pressure-time histories from the four ignited tests. Skjold (2018a,b) describes the procedures for data processing and filtering in detail. The vertical dash-dotted lines indicate the degree of opening for the hinged vent panels. Fig. 17 shows selected frames from test 61: *a)* when the vent panels start to open (t_{stat}), *b-e)* when the vent panels are approximately 45°, 90°, 180° and 270° open, and after the test *f)*. For simplicity, and because of significant drift in some of the signals, the plots show only one pressure-time curve for each pair of symmetrically placed pressure sensors (Fig. 9). The final report from the HySEA experiments in 20-foot containers includes the pressure-time histories for all the 66 vented deflagration tests (Skjold, 2018b). Overall, the overpressures increase somewhat with the introduction of the pipe rack (P2). The highest pressures are obtained for pressure transducer P7 in test 61. As shown in Fig. 15, this is the only ignited test where the measured hydrogen concentrations were at the same level as in the unignited tests.

4. Consequence models

This section introduces the models used by the modellers that participated in the blind-prediction benchmark study.

4.1. Empirical and semi-empirical models

Table 3 summarises the models based on empirical or semi-empirical correlations. The calculation time for a given scenario is insignificant for this category of models, but none of the models accounts for the effect of stratification. Hence, the model predictions assume homogeneous mixtures with different concentrations. For the sake of brevity, the models are not described in detail in this paper, but references to standards or publications are provided for all models. Since all model predictions in this category were submitted by the same group, it is reasonable to assume consistent use of model parameters. The results for the modified External Cloud Model (ECM-II) were submitted after the tests had been performed.

The University of Warwick developed the ECM models as part of the HySEA project (Sinha et al., 2019a,b; Sinha and Wen, 2019). Several aspects of the ECM models are inspired by and resemble the models developed by FM Global (Bauwens et al., 2012), including a physics-based approach for estimating the maximum pressure during vented deflagrations. Both models include simplified versions based on tabulated bulk parameters for engineering calculations. However, several aspects of the models are different, and a detailed comparison is outside the scope of the present paper.

4.2. CFD tools

Table 4 summarises the CFD-based consequence models. The calculation time for a given scenario can vary from less than an hour to several days. For the sake of brevity, the model descriptions focus on version numbers, grid resolution, CFL numbers used, and similar parameters. The model predictions will also depend on other factors, including how the modeller implements the geometry and how the computational mesh (grid) is defined relative to the geometry. For technical details, please refer to the respective user manuals and cited publications.

5. Model predictions

This section summarises the comparison between experimental results and model predictions.

5.1. Release and dispersion

Fig. 18 shows the experimental and predicted hydrogen concentration profiles at the time of ignition. Several of the model predictions captured the stratification reasonably well, but some did not. For prediction M1a, all monitor points were placed relative to the ground, and not relative to the floor inside the container (i.e. about 0.5 m below the actual measurements). The corrected values (M1b) capture the stratification reasonably well. The results reported for M3 and M6 do not indicate any significant stratification. Insufficient refinement of the grid near the release point can explain the results for M6. For prediction M7, the actual CFD simulation (M7a) captured the stratification, but the concentrations were diluted with air from the outside when the simulated cloud was transferred to coarser grids that did not coincide with the walls of the enclosure (M7b, M7c, and M7d).

Fig. 19 compares model predictions (lines), and experimental results (points), for hydrogen concentration in the positions indicated in Fig. 10 for test configurations with frame only (FO) and pipe rack in the centre position (P2). The overall results are similar for tests with and without the pipe rack. The experimental values indicated for position A4′ (FO) in Fig. 19 are most likely erroneous, possibly due to a leak in

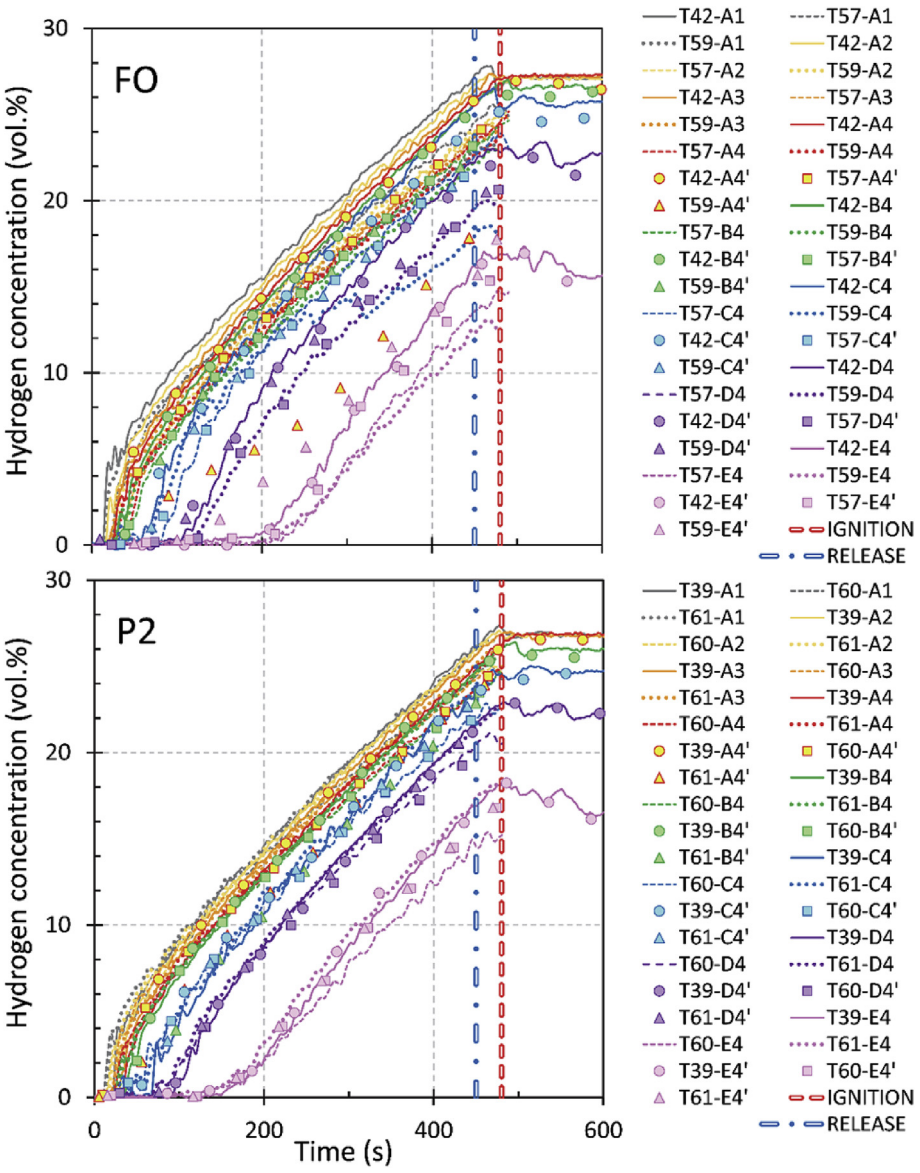

Fig. 15. Hydrogen concentrations for unignited and ignited tests for both scenarios (FO and P2).

the sampling tube.

5.2. Vented explosions

Fig. 20 and Fig. 21 compare the pressure-time histories from experiments and CFD simulations. In general, predictions M1 and M5-M7, all using the CFD tool FLACS, significantly over-predict the explosion pressure, whereas the other CFD codes M2-M4 under-predict the pressures.

Fig. 22 summarises the maximum overpressure and corresponding pressure impulse predicted by the various modellers for both scenarios. The results reported by M6 and M7 reveal a significant effect of grid resolution, including opposite trends with and without the pipe rack (M6).

Fig. 23 summarises the maximum overpressures predicted by the engineering models for both scenarios, assuming various homogeneous hydrogen concentrations inside the container. The results show less variability than the predictions obtained with the CFD tools.

6. Discussion

The two scenarios selected for the second blind-prediction benchmark study in the HySEA project were quite challenging from a modelling point of view. A 'perfect' model should be able to predict the stratification of hydrogen during the release, the transient flame propagation through the inhomogeneous mixture and the pipe rack obstacle, and finally the structural response of the vent panels and the relatively weak enclosure. However, the application areas for the models represented in the blind-prediction study include design optimisation and risk assessments for industrial facilities, which typically involve an even broader range of spatial scales and significantly more complex geometries. As such, the results from the second blind-prediction benchmark study in the HySEA project provide a realistic measure of the level of accuracy or variability that can be expected from this type of engineering calculations.

6.1. Measurement uncertainty and repeatability of experiments

The concentration measurements summarised in Fig. 15 and 18 indicate moderate loss of fuel before ignition for tests 57, 59 and 60,

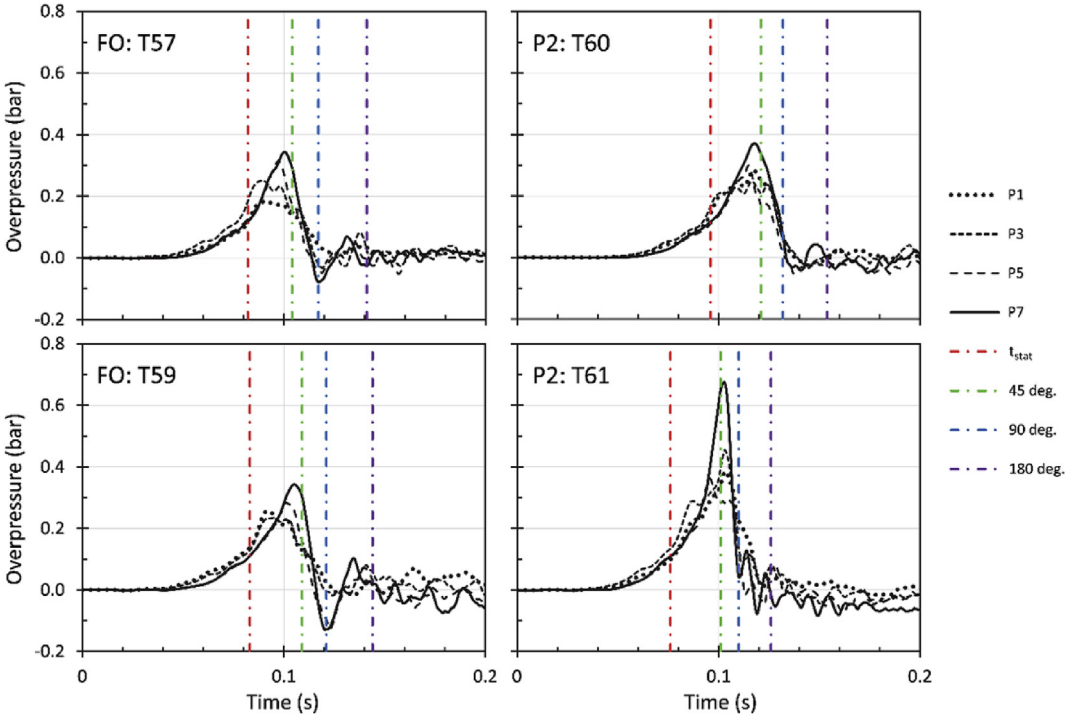

Fig. 16. Experimental pressure-time histories.

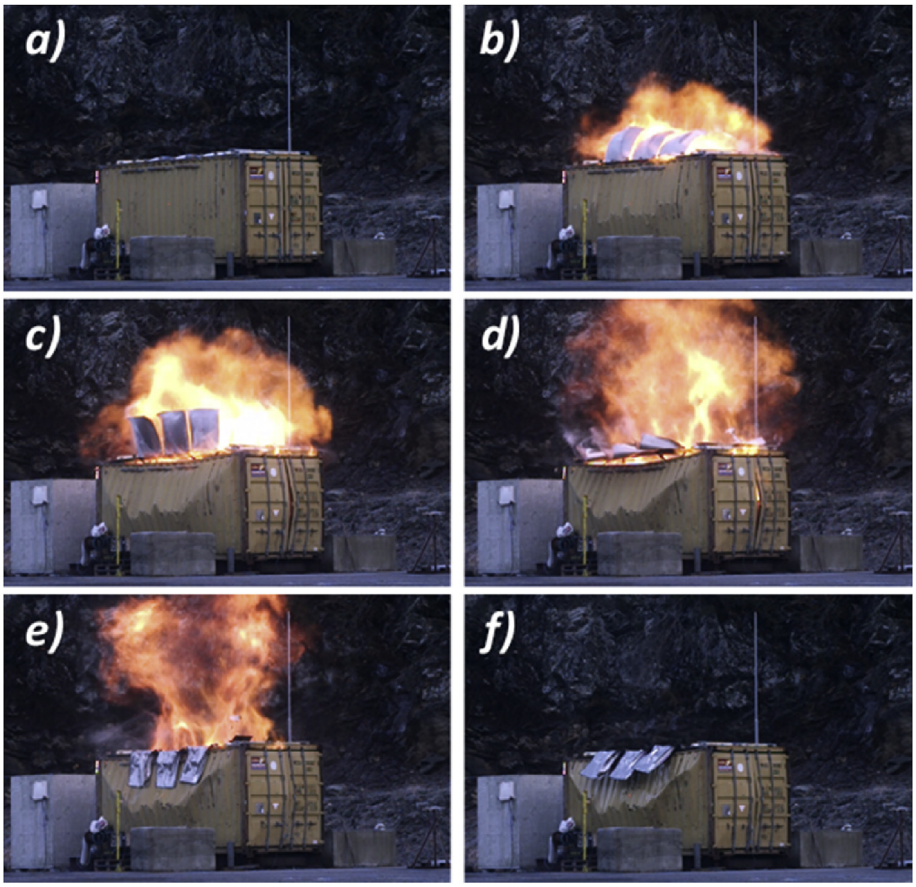

Fig. 17. Opening of vent panels for test 61.

Table 3
Empirical and semi-empirical models.

Modeller	Model	Reference	Assumptions
M-8	EN 14994	EN 14994 (2007)	Homogeneous: 21 or 25 vol.% hydrogen in air.
M-8	NFPA-68	NFPA-68 (2013)	Homogeneous: 21 or 25 vol.% hydrogen in air.
M-8	FM Global	Bauwens et al. (2012)	Homogeneous: 21 or 25 vol.% hydrogen in air.
M-8	Molkov	Molkov and Bragin (2015)	Homogeneous: 21 or 25 vol.% hydrogen in air.
M-8	ECM-I	Sinha et al. (2018), Sinha and Wen (2018)	Homogeneous: 21 or 25 vol.% hydrogen in air.
M-8	ECM-II	Sinha et al. (2019a,b), Sinha and Wen (2019)	Homogeneous: 24 vol.% hydrogen in air.

possibly combined with the somewhat lower mass flow in the releases for test 57 and 59 (Fig. 13). This observation is consistent with the higher explosion pressures and more severe wall deflection measured in test 61, compared to test 60 (Table 2 and Fig. 16). Hence, the effect of introducing the pipe rack (P2) may not be as pronounced as indicated in Fig. 22 and 23, since the pressures measured without the pipe rack (FO) probably would have been somewhat higher without loss of fuel. As mentioned in section 3.2, the uncertainty related to the pressure sensors is negligible compared to the variability associated with temperature drift, smoothing during post-processing, and the inherent spread in results between repeated tests (tests 60 and 61 in Fig. 16). Compared to the tests with stratified mixtures, the reference tests with homogeneous mixtures show less variation. However, this can be somewhat misleading since only test 39 involved homogeneous mixture and obstacle configuration P2 (Table 1). Additional repeated tests would presumably have resulted in a wider spread in the experimental results.

6.2. Model uncertainty and user dependence for CFD models

The long-duration releases from a relatively small opening and gradual stratification in a large enclosure implied time-consuming simulations for the CFD codes summarised in Table 4. The varying degree of accuracy in the predictions of the concentration field inside the container implies that the initial conditions used for the vented deflagration simulations varied significantly between the various models. Nevertheless, Fig. 18 shows that several modellers predicted the stratification inside the container reasonably well (M1b, M4, M5, and M7a), given the inherent uncertainty in the experimental results (Fig. 13 and 15). User errors explain several of the deviations between model predictions and experimental results, including misplaced monitor points (M1a), insufficient refinement of the jet release (M6), and inconsistent transformation of results from one computational grid to coarser grid resolutions (M7bcd). Measures such as automated gridding, improved training, better user documentation and certification of users can improve the accuracy of the model predictions significantly.

The use of a relatively coarse mesh for the dispersion simulations is the primary explanation for the reduced overall concentration and lack of stratification in the prediction with HyFOAM (M3 in Fig. 18). Limited spatial resolution resulted in excess diffusion of hydrogen, rapid mixing, and hence minimal stratification (similar to prediction M6). Furthermore, to reduce the simulation time, the computational mesh covered only the interior of the container, and atmospheric boundary conditions were applied for the 20 holes along the walls. This approach resulted in pressure gradients inside the enclosure during the release, discharge of hydrogen, and lower fuel concentrations.

Significant deviations in the prediction of the concentration field in the flammable cloud will inevitably influence the predictions for the maximum reduced explosion pressure. As such, it is not straightforward to interpret the significant spread in maximum explosion pressure and

Table 4
Overview of the CFD tools used in the blind-prediction benchmark study.

Modeller	Model description
M-1	***FLACS v10.6 r3*** (Gexcon, 2018) Release and dispersion simulations with 0.10 m grid cells, local refinement near leak (0.016 m), and variable CFL conditions. The explosion simulations used 0.10 m uniform grid with initial conditions from dispersion simulation after 480 s. Pressure relief panels modelled as pop-out panels with activation pressure 0.10 bar.
M-2	***Fluidyn*** Minimum grid resolution 0.007 m (FO) and 0.00092 m (P2). Computational time steps 0.1 s for the release scenarios and 0.00005 s for the explosion scenarios. The simulation used a symmetry plane, standard k-ε turbulence model and the modified Bray–Moss–Libby (BML) combustion model with single-step reactions.
M-3	***HyFOAM*** (Rao and Wen, 2019) Large eddy simulation (LES) solver developed within the OpenFOAM framework. Flame wrinkling combustion model with additional sub-models to account for flame instabilities in lean hydrogen-air mixtures deflagrations, including Lewis number effects.
M-4	***ADREA-HF*** (Venetsanos et al., 2010) Symmetry plane, standard k-ε turbulence model with additional buoyancy terms and ideal gas assumption. Release and dispersion simulations with inlet resolved by two cells (minimum size 0.009 m), and CFL = 40 (time step = 0.015 s during release), and total number of cells 664 576 and 912 789 for the FO and P2 case, respectively. Combustion simulations with approximately uniform grid (0.05 m cell size) inside the enclosure for the FO case, refinement to 0.03 m in non-vertical directions for the obstacle in the P2 case, Yakhot equation for turbulent burning velocity, modifications to account for flame instabilities, and total number of cells 1 758 120 and 1 919 580 for the FO and P2 case, respectively. All the six vent panels were assumed to open instantaneously and simultaneously when the overpressure at the position of the middle pair of panels reached 0.1 bar.
M-5	***FLACS v10.6 r3*** (Gexcon, 2018) Release and dispersion scenarios modelled with compressible solver and CFLV = 2 for efficient calculations. Base grid for dispersion 0.20 m in horizontal and 0.10 m in the vertical direction, automatic refinement around leak (0.018 m) and 0.05 m vertical in the lower part of the enclosure. Explosion simulations with 0.10 m grid resolution inside the container and outside vent, and 0.20 m outside the container. A sensitivity study on panel weight and the effective opening area indicated a limited impact on simulation results.
M-6	***FLACS v10.6 r3*** (Gexcon, 2018) Release and dispersion simulations with 0.07 m grid cells and local refinement near leak (0.045 m), and 0.06 (a), 0.07 (b), 0.08 (c) and 0.10 m (d) grid cells for explosion simulations. Boundary conditions: NOZZLE for dispersion cases and PLANE WAVE for explosion cases. The density of hydrogen used for converting between mass and volume flow assumed ambient temperature of 15 °C.
M-7	***FLACS 10.2*** (Gexcon, 2018) Grid resolution 0.10 m (a) for dispersion simulations, and conversion of the resulting cloud to coarser meshes (b-d) using the rd-file utility in FLACS. Grid resolution 0.10 (a), 0.15 (b), 0.20 (c) and 0.30 m (d) for explosion simulations. Dispersion simulations used CFLV = 5 and CFLC = 125, and explosion simulations used CFLV = 0.5 and CFLC = 5.

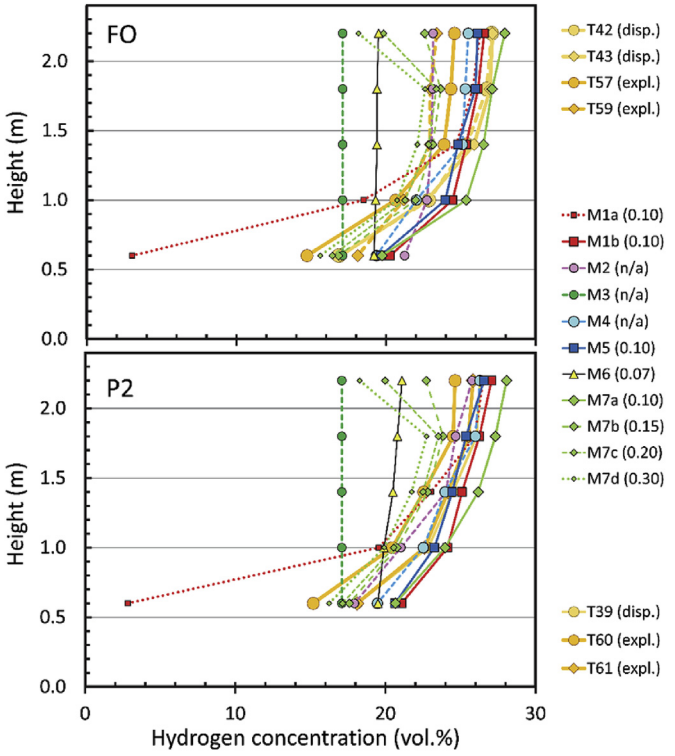

Fig. 18. Concentration profiles at the time of ignition.

impulse for model predictions M6 (abcd) and M7 (bcd). The results from the CFD simulations vary significantly with grid resolution. Since it is not straightforward to obtain grid convergence for porosity/distributed resistance (PDR) models, such as FLACS, a short-term solution for users of the software may entail updated grid guidelines for scenarios with highly reactive fuels, such as hydrogen.

It is not straightforward to predict the effect of the coupling between the moving walls and the propagating flame on the rate of combustion and pressure build-up inside the enclosure. None of the models listed in Table 4 includes the effect of the structural response of weak enclosures, such as shipping containers. Significant deflection of the container walls increases the volume of the enclosure, which may result in lower explosion pressures compared to a rigid structure (Rao and Wen, 2018; Atanga et al., 2019). Fig. 17 illustrates how significant deformation of the walls creates additional openings in the container, such as the gap between the upper edge of the side walls and the steel frame supporting the vent panels. The severe bulging of the doors in test 61 also resulted in a temporary opening. However, the pressure-time histories in Fig. 16 show that the maximum pressure is reached by the time the vent panels are approximately 45° open (Fig. 17b), which may indicate that the effect of two-way coupling between combustion and structural response is limited for these tests.

The values for P_{stat} in Table 2 indicate that the vent panels opened consistently in all tests, and Fig. 16 shows that the maximum reduced explosion pressures occurred when the vent panels had opened approximately 45°. Hence, the most critical part of the venting process took place well before the panels were fully open. None of the three models that under-predict the explosion pressure in Fig. 22 (M2, M3, and M4) considered the actual opening time and movement of the vent panels. The areas covered by the panels were treated as closed until the internal pressure reached a static opening pressure of 0.1 bar, and thereafter as fully open. This modelling approach results in an ideal venting device, which hardly can be realised in practice, and this is likely to have contributed significantly to the under-prediction of P_{max}. The CFD tool FLACS (M1, M5, M6 and M7) includes sub-grid models for various types of venting devices, including hinged panels. However, investigations conducted in the aftermath of the blind-prediction study revealed that the results are quite sensitive to the representation of the vent panels, including the dynamic response of the panels. Future modelling work should focus on improving the representation of realistic explosion venting devices in CFD tools (EN 14797, 2006).

6.3. Model uncertainty and user dependence for empirical and semi-empirical models

None of the simplified models summarised in Table 3 includes the effect of stratification. Hence, it was only possible to investigate the effect of varying the fuel concentration throughout the enclosure. Makarov et al. (2018) have proposed a model for inhomogeneous hydrogen-air mixtures, but this model was not included in the blind-prediction study.

Compared to the predictions obtained with CFD tools (Fig. 22), the predictions obtained with the empirical and semi-empirical models show less variation (Fig. 23). This observation is hardly surprising, since the geometry of a 20-foot shipping container is relatively simple, and the same group submitted all the predictions with simple models. As such, the results in Fig. 23 do not include any variation between different modellers using the same model. Furthermore, the stratification of hydrogen inside the container resulted in a highly reactive layer beneath the ceiling, and limited effect of the internal pipe rack obstacle on flame propagation and pressure build-up in the experiments. The effect of stratification is evident in the experimental results and should be accounted for by empirical or semi-empirical models for vented hydrogen deflagrations.

Since containers used for hydrogen energy applications usually contain various types of equipment, and the presence of obstacles can have pronounced effect on flame acceleration and pressure build-up (Skjold et al., 2019b), empirical or semi-empirical models for vented deflagrations in weak enclosures should account for the effect on internal geometry. However, it is not straightforward to include the effect of complex geometry in simple models, and Fig. 23 shows that only three of the simple models predict a noticeable effect of the obstacle (Bauwens et al., 2012; Molkov and Bragin, 2015; Sinha et al., 2019a,b; Sinha and Wen, 2019). The latest edition of the NFPA standard also include the effect of obstacles (NFPA 68, 2018), but this model was not included in the blind-prediction study. In summary, there is significant potential for improving the performance of simplified models for vented hydrogen deflagrations (Lakshmipathy et al., 2019).

6.4. Implications and suggestions for further work

It is foreseen that the increasing demand for sustainable energy solutions will result in increased use of hydrogen as an energy carrier in society. Since fires and explosions represent a significant hazard for most hydrogen installations, specific measures are often required for reducing the risk to a tolerable level. Both quantitative risk assessments (QRAs) and optimal design of hydrogen installations require reliable and reasonably accurate consequence models. However, some specific properties of hydrogen complicate the modelling of vented deflagrations significantly. Hydrogen is highly reactive, and flames in lean hydrogen-air mixtures are inherently unstable. Loss of containment in a confined space is likely to result in a stratified mixture that, if ignited, can produce significantly higher explosion pressures compared to a lean homogeneous mixture containing the same amount of hydrogen.

Regardless of the uncertainty and inherent variability in the experimental results, the significant spread in model predictions and the deviations between model predictions and experiments suggest that there is considerable potential for improving the models for vented hydrogen deflagrations. The large spread in the predictions by modellers using the same CFD tool demonstrates a need for improved documentation and training for users. The variability can also be reduced by implementing automated and carefully validated procedures

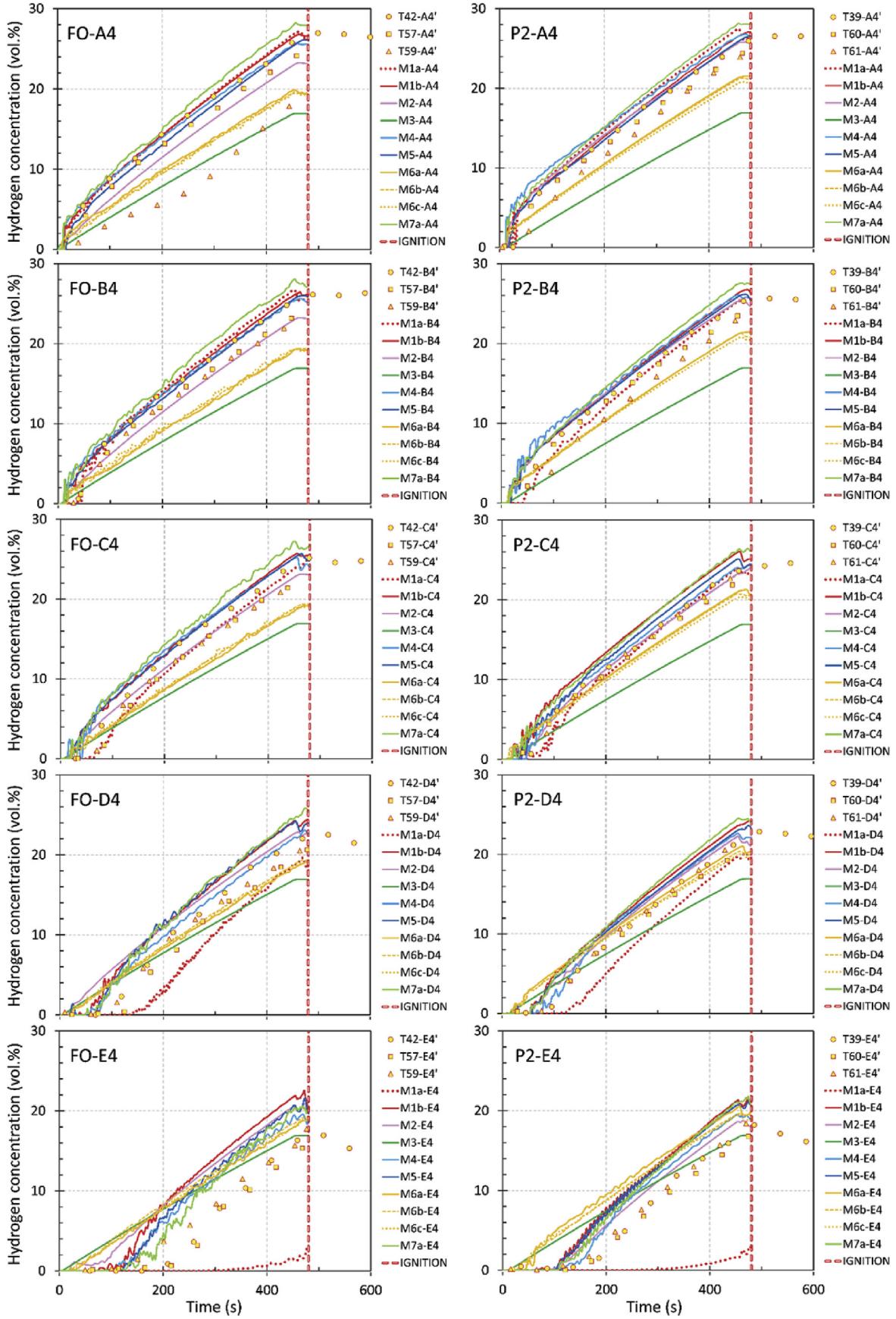

Fig. 19. Model predictions for hydrogen dispersion with frame only (FO) and pipe rack (P2).

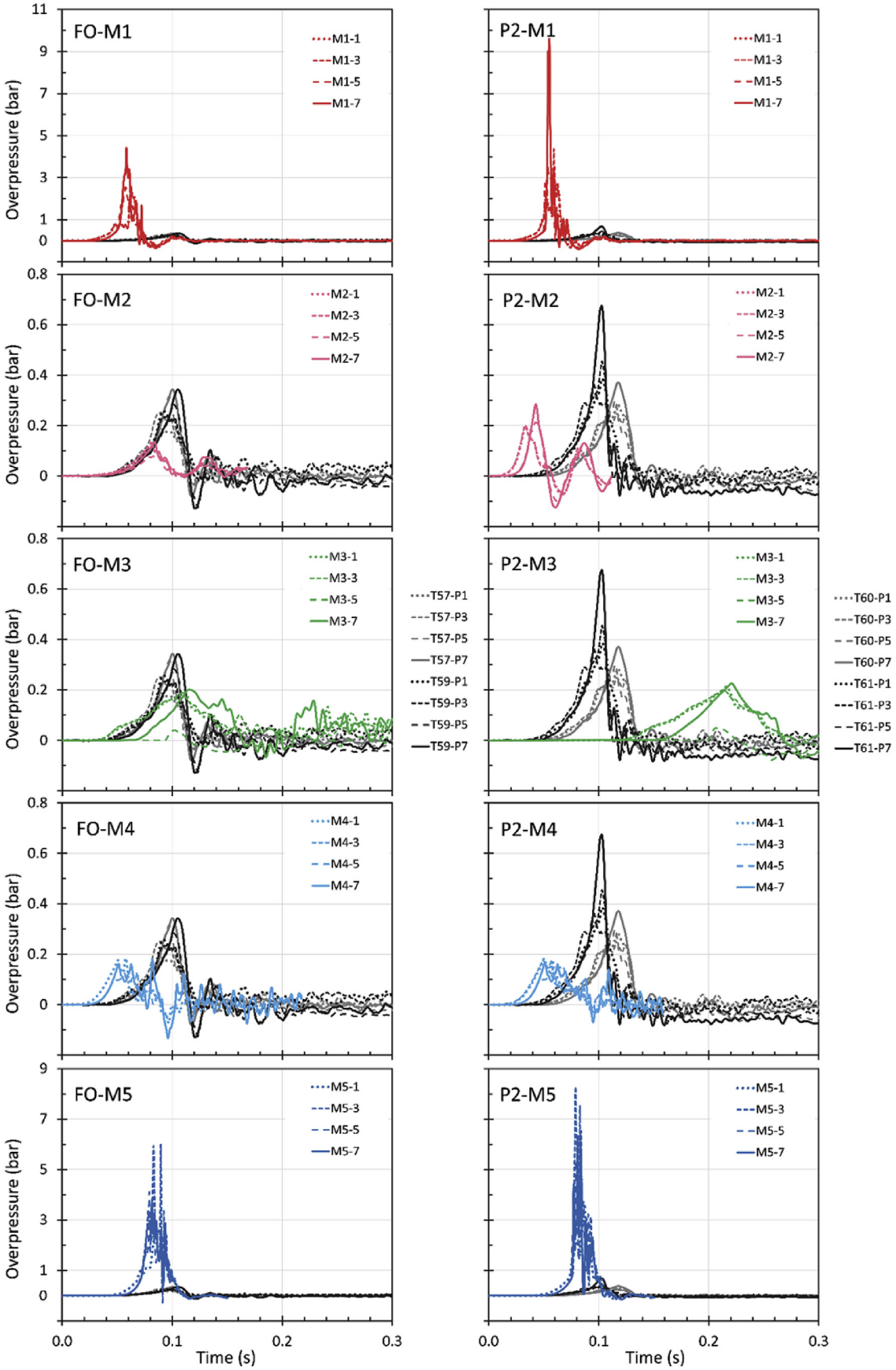

Fig. 20. Predicted pressure-time histories for models M1-M5.

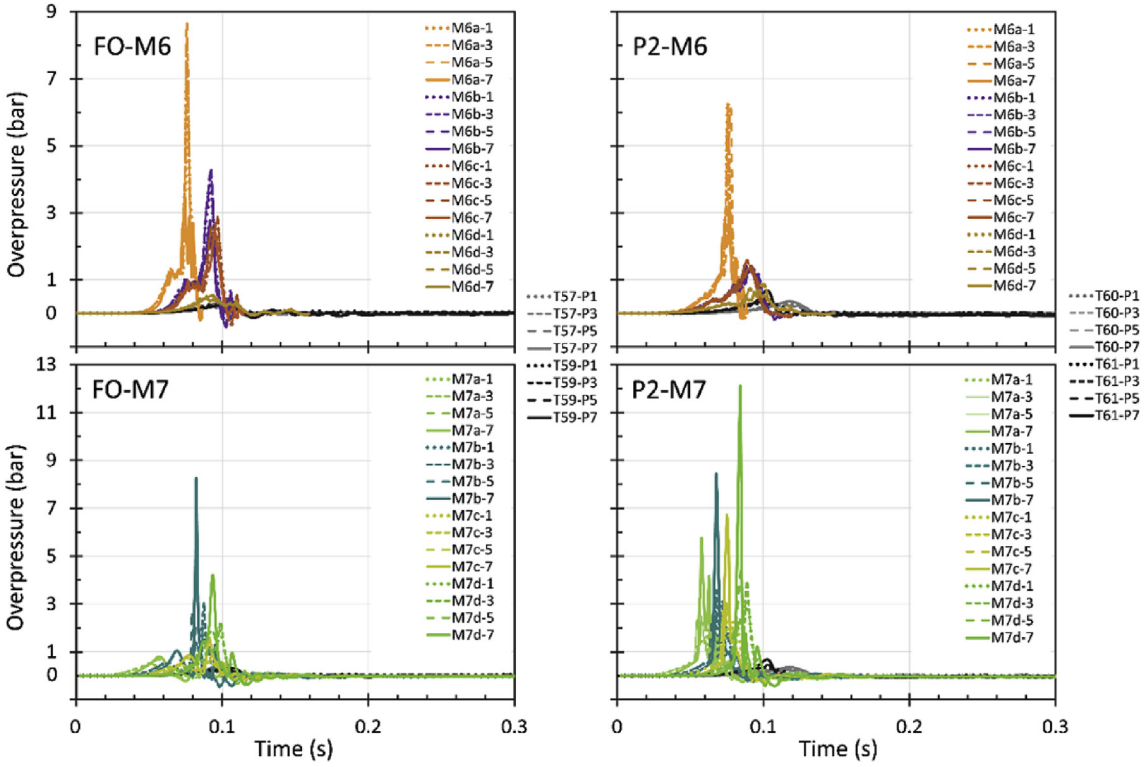

Fig. 21. Predicted pressure-time histories for models M6 and M7.

for setting up simulations, including the generation of the computational mesh.

It is essential for safety engineers to be aware of the inherent limitations of the model systems they use, and to critically evaluate the model predictions considering available experiments and documented model performance from systematic validation studies (Skjold et al., 2013; Tolias et al., 2018). Further blind-prediction benchmark studies for realistic accident scenarios in full-scale geometries is required for documenting the predictive capabilities of models and modellers, and hence the inherent uncertainty associated with risk assessments for hydrogen installations in industry and society in general.

7. Conclusions

The second blind-prediction benchmark study in the HySEA project explored a two-stage chain of events, starting with release and dispersion of hydrogen inside a 20-foot ISO container, followed by vented deflagrations. Although several modellers predicted the stratification of hydrogen inside the container with reasonable accuracy, the large spread in results for the maximum reduced explosion pressure suggests that the scenarios represented a significant challenge for modellers. It is foreseen that the blind-prediction benchmark exercises performed as part of the HySEA project will contribute to increased awareness amongst developers and users of advanced consequence models, as well as model improvements and updated documentation and guidelines.

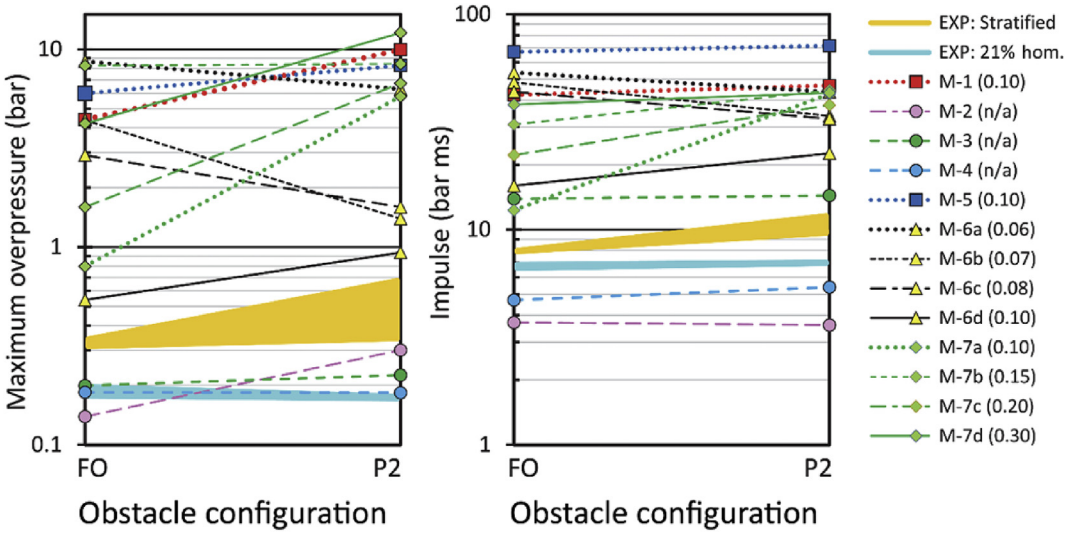

Fig. 22. Summary of results for the CFD tools.

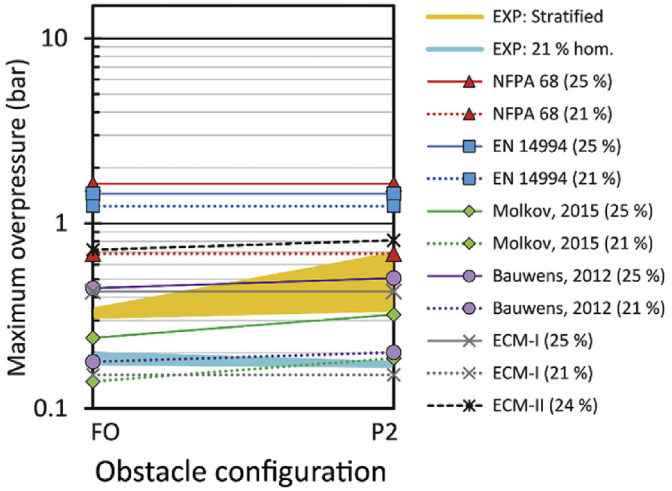

Fig. 23. Summary of results for the empirical and semi-empirical models.

Disclaimer

A part of this work was co-funded by the Health and Safety Executive (HSE). The contents of the publication, including any opinions and conclusions expressed are those of the authors alone and do not necessarily reflect HSE policy. The same applies to the contributions from the other organisations.

Acknowledgements

The HySEA project received funding from the Fuel Cells and Hydrogen 2 Joint Undertaking (FCH 2 JU) under grant agreement No 671461. This Joint Undertaking received support from the European Union's Horizon 2020 research and innovation programme and the United Kingdom, Italy, Belgium and Norway. The members of the HySEA consortium gratefully acknowledge the valuable contributions from the members of the HySEA Advisory Board: Simon Jallais and Elena Vyazmina from Air Liquide, Derek Miller from Air Products, Carl Regis Bauwens from FM Global and Y.F. (John) Khalil from United Technologies Research Center (UTRC).

Appendix A. Supplementary data

Supplementary data to this article can be found online at https://doi.org/10.1016/j.jlp.2019.06.013.

References

Astbury, G.R., 2008. A review of the properties and hazards of some alternative fuels. Process Saf. Environ. Protect. 86, 397–414.

Atanga, G., Lakshmipathy, S., Skjold, T., Hisken, H., Hanssen, A.G., 2019. Structural response for vented hydrogen deflagrations: coupling CFD and FE tools. Int. J. Hydrogen Energy 44, 8893–8903. https://doi.org/10.1016/j.ijhydene.2018.08.085.

Baraldi, D., Kotchourko, A., Lelyakin, A., Yanez, J., Gavrikov, A., Efimenko, A., Verbecke, F., Makarov, D., Molkov, V., Teodorczyk, A., 2010. An inter-comparison exercise on CFD model capabilities to simulate hydrogen deflagrations with pressure relief vents. Int. J. Hydrogen Energy 35, 12381–12390.

Baraldi, D., Melideo, D., Kotchourko, A., Ren, K., Yanez, J., Jedicke, O., Giannissi, S.G., Tolias, I.C., Venetsanos, A.G., Keenan, J., Makarov, D., Molkov, V., Slater, S., Verbecke, F., Duclos, A., 2017. Development of a model evaluation protocol for CFD analysis of hydrogen safety issues the SUSANA project. Int. J. Hydrogen Energy 42, 7633–7643.

Bauwens, C.R., Dorofeev, S.B., 2014. Effect of initial turbulence on vented explosion overpressures from lean hydrogen-air deflagrations. Int. J. Hydrogen Energy 39, 20509–20515.

Bauwens, C.R., Chaffee, J., Dorofeev, S.B., 2011. Vented explosion overpressures from combustion of hydrogen and hydrocarbon mixtures. Int. J. Hydrogen Energy 36, 2329–2336.

Bauwens, C.R., Chao, J., Dorofeev, S.B., 2012. Effect of hydrogen concentration on vented explosion overpressures from lean hydrogen-air deflagrations. Int. J. Hydrogen Energy 37, 17599–17605.

Ciccarelli, G., Dorofeev, S.B., 2008. Flame acceleration and transition to detonation in ducts. Prog. Energy Combust. Sci. 34, 499–550.

Clavin, P., Searby, G., 2016. Combustion Waves and Fronts in Flows. Cambridge University Press, Cambridge.

Crowl, D.A., Jo, Y.-D., 2007. The hazard and risks of hydrogen. J. Loss Prev. Process. Ind. 20, 158–164.

Dorofeev, S.B., Kochurko, A.S., Efimenko, A.A., Chaivanov, B.B., 1994. Evaluation of the hydrogen explosion hazard. Nucl. Eng. Des. 148, 305–316.

EN 14797, 2006. Explosion Venting Devices. European Committee for Standardization (CEN), Brussels, Belgium 30 pp.

EN 14994, 2007. Gas Explosion Venting Protective Systems. European Committee for Standardization (CEN), Brussels, Belgium 30 pp.

Evans, J.A., Exon, R., Johnson, D.M., 1999. The Repeatability of Large Scale Explosion Experiments. UK Health & Safety Executive (HSE) Offshore Technology Report, OTO 1999 042, October 1999.

Fuster, B., Houssin-Agbomson, D., Jallais, S., Vyazmina, E., Dang-Nhu, G., Bernard-Michel, G., Kuznetsov, M., Molkov, V., Chernyavskiy, B., Shentsov, V., Makarov, D., Dey, R., Hooker, P., Baraldi, D., Weidner, E., Melideo, D., Palmisano, V., Venetsanos, A., Kinderen, J.D., 2017. Guidelines and recommendations for indoor use of fuel cells and hydrogen systems. Int. J. Hydrogen Energy 2, 7600–7607.

García, J., Baraldi, D., Gallego, E., Beccantini, A., Crespo, A., Hansen, O.R., Høiset, S., Kotchourko, A., Makarov, D., Migoya, E., Molkov, V., Voort, M.M., Yanez, J., 2010. An intercomparison exercise on the capabilities of CFD models to reproduce a large-scale hydrogen deflagration in open atmosphere. Int. J. Hydrogen Energy 35, 4435–4444.

Gallego, E., Migoya, E., Martín-Valdepeñasa, J.M., Crespo, A., García, J., Venetsanos, A., Papanikolaou, E., Kumar, S., Studer, E., Dagba, Y., Jordan, T., Jahn, W., Høiset, S., Makarov, D., Piechna, J., 2007. An intercomparison exercise on the capabilities of CFD models to predict distribution and mixing of H_2 in a closed vessel. Int. J. Hydrogen Energy 32, 2235–2245.

Gexcon, 2018. FLACS User's Manual v10.6 R3. Gexcon, Bergen.

Hooker, P., Hoyes, J.R., Willoughby, D., 2017. Experimental studies of vented deflagrations in a low strength enclosure. Int. J. Hydrogen Energy 42, 7565–7576.

Konnov, A.A., Mohammad, A., Kishore, V.R., Kim, N.I., Prathap, C., Kumar, S., 2018. A comprehensive review of measurements and data analysis of laminar burning velocities for various fuel+air mixtures. Prog. Energy Combust. Sci. 68, 197–267.

Lakshmipathy, S., Skjold, T., Hisken, H., Atanga, G., 2019. Consequence models for vented hydrogen deflagrations: CFD vs. engineering models. Int. J. Hydrogen Energy 44, 8699–8710. https://doi.org/10.1016/j.ijhydene.2018.08.079.

Makarov, D., Verbecke, F., Molkov, V., Roe, O., Skotenne, M., Kotchourko, A., Lelyakin, A., Yanez, J., Hansen, O., Middha, P., Ledin, S., Baraldi, D., Heitsch, M., Efimenko, A., Gavrikov, A., 2009. An inter-comparison exercise on CFD model capabilities to predict a hydrogen explosion in a simulated vehicle refuelling environment. Int. J. Hydrogen Energy 34, 2800–2814.

Makarov, D., Hooker, P., Kuznetsov, M., Molkov, V., 2018. Deflagrations of localised homogeneous and inhomogeneous hydrogen-air mixtures in enclosures. Int. J. Hydrogen Energy 4 (3), 9848–9869.

Molkov, V., Bragin, M., 2015. Hydrogen-air deflagrations: vent sizing correlation for low-strength equipment and buildings. Int. J. Hydrogen Energy 40, 1256–1266.

Moradi, R., Groth, K.M., 2019. Hydrogen storage and delivery: review of the state of the art technologies and risk and reliability analysis. Int. J. Hydrogen Energy 44, 12254–12269.

NFPA 68, 2013. Standard on Explosion Protection by Deflagration Venting. National Fire Protection Association (NFPA), Quincy, Massachusetts978-145590622-2.

NFPA 68, 2018. Standard on Explosion Protection by Deflagration Venting. National Fire Protection Association (NFPA), Quincy, Massachusetts978-145591896-6.

Ono, R., Nifuku, M., Fujiwara, S., Horiguchi, S., Oda, T., 2007. Minimum ignition energy of hydrogen-air mixture: effects of humidity and spark duration. J. Electrost. 65, 87–93.

Razus, D.M., Krause, U., 2001. Comparison of empirical and semi-empirical calculation methods for venting of gas explosions. Fire Saf. J. 36, 1–23.

Rao, V.C.M., Wen, J.X., 2018. Fluid structure interactions modelling in vented lean deflagrations. In: Proceedings Twelfth International Symposium on Hazards, Prevention and Mitigation of Industrial Explosions (XII ISHPMIE). 978-1-5323-8443-1, pp. 899–914. Kansas City, 12-17 August 2018. https://doi.org/10.5281/zenodo.2602154.

Rao, V.C.M., Wen, J.X., 2019. Numerical modelling of vented lean hydrogen deflagrations in an ISO container. Int. J. Hydrogen Energy 44, 8767–8779.

Rigas, F., Amyotte, P., 2013. Myths and facts about hydrogen hazards. Chem. Eng. Trans. 31, 913–918.

Sánchez, A.L., Williams, F.A., 2014. Recent advances in understanding of flammability characteristics of hydrogen. Prog. Energy Combust. Sci. 41, 1–55.

Sinha, A., Rao, V.C.M., Wen, J.X., 2018. Comparison of engineering and CFD model predictions for overpressures in vented explosions. In: Proceedings Twelfth International Symposium on Hazards, Prevention and Mitigation of Industrial Explosions (XII ISHPMIE). 978-1-5323-8443-1, pp. 860–874. Kansas City, 12-17 August 2018. https://doi.org/10.5281/zenodo.2600350.

Sinha, A., Wen, J.X., 2018. Phenomenological modelling of external cloud formation in vented explosions. In: Proceedings Twelfth International Symposium on Hazards, Prevention and Mitigation of Industrial Explosions (XII ISHPMIE). 978-1-5323-8443-1, pp. 847–859. Kansas City, 12-17 August 2018. https://doi.org/10.5281/zenodo.2601952.

Sinha, A., Rao, V.C.M., Wen, J.X., 2019a. Modular phenomenological model for vented explosions and its validation with experimental and computational results. J. Loss Prev. Process. Ind (in press). https://doi.org/10.1016/j.jlp.2019.05.017.

Sinha, A., Rao, V.C.M., Wen, J.X., 2019b. Performance evaluation of empirical models for

vented lean hydrogen explosions. Int. J. Hydrogen Energy 44, 8711–8726. https://doi.org/10.1016/j.ijhydene.2018.09.101.

Sinha, A., Wen, J.X., 2019. A simple model for calculating peak pressure in vented explosions of hydrogen and hydrocarbons. Int. J. Hydrogen Energy (in press). https://doi.org/10.1016/j.ijhydene.2019.02.213.

Skjold, T., 2018a. Vented hydrogen deflagrations in 20-foot ISO containers. In: Proceedings Twelfth International Symposium on Hazards, Prevention and Mitigation of Industrial Explosions (XII ISHPMIE). 978-1-5323-8443-1, pp. 823–846. Kansas City, 12-17 August 2018. https://doi.org/10.5281/zenodo.2603985.

Skjold, T., 2018b. Experimental Investigation of Vented Hydrogen Deflagrations in Containers: Homogeneous and Inhomogeneous Mixtures. Report HySEA-D2-08-2018: 638 pp.

Skjold, T., Hisken, H., Lakshmipathy, S., Atanga, G., Carcassi, M., Schiavetti, M., Stewart, J.R., Newton, A., Hoyes, J.R., Tolias, I.C., Venetsanos, A.G., Hansen, O.R., Geng, J., Huser, A., Helland, S., Jambut, R., Ren, K., Kotchourko, A., Jordan, T., Daubech, J., Lecocq, G., Hanssen, A.G., Kumar, C., Krumenacker, L., Jallais, S., Miller, D., Bauwens, C.R., 2019a. Blind-prediction: estimating the consequences of vented hydrogen deflagrations for homogeneous mixtures in 20-foot ISO containers. Int. J. Hydrogen Energy 44, 8997–9008. https://doi.org/10.1016/j.ijhydene.2018.06.191.

Skjold, T., Hisken, H., Lakshmipathy, S., Atanga, G., van Wingerden, M., Olsen, K.L., Holme, M.N., Turøy, N.M., Mykleby, M., van Wingerden, K., 2019b. Vented hydrogen deflagrations in containers: effect of congestion for homogeneous and inhomogeneous mixtures. Int. J. Hydrogen Energy 44, 8819–8832. https://doi.org/10.1016/j.ijhydene.2018.10.010.

Skjold, T., Pedersen, H.H., Bernard, L., Middha, P., Narasimhamurthy, V.D., Landvik, T., Lea, T., Pesch, L., 2013. A matter of life and death: validating, qualifying and documenting models for simulating flow-related accident scenarios in the process industry. Chem. Eng. Trans. 31, 187–192.

Skjold, T., Siccama, D., Hisken, H., Brambilla, A., Middha, P., Groth, K.M., LaFleur, A.C., 2017. 3D risk management for hydrogen installations. Int. J. Hydrogen Energy 42, 7721–7730.

Skjold, T., Souprayen, C., Dorofeev, S., 2018. Perspective: fires and explosions. Prog. Energy Combust. Sci. 64, 2–3.

Sommersel, O.K., Bjerketvedt, D., Christensen, S., Krest, O., Vaagsaether, K., 2008. Application of background oriented Schlieren for quantitative measurements of shock waves from explosions. Shock Waves 18, 291–297. https://doi.org/10.1007/s00193-008-0142-1.

Sommersel, O.K., Vaagsaether, K., Bjerketvedt, D., 2017. Hydrogen explosions in 20′ ISO container. Int. J. Hydrogen Energy 42, 7740–7748. https://doi.org/10.1016/j.ijhydene.2016.06.239.

Sustek, J., Janovsky, B., 2013. Comparison of empirical and semi-empirical equations for vented gas explosion with experimental data. J. Loss Prev. Process. Ind. 26, 1549–1557. https://doi.org/10.1016/j.jlp.2013.08.014.

Tolias, I.C., Giannissi, S.G., Venetsanos, A.G., Keenan, J., Shentsov, V., Makarov, D., Coldrick, S., Kotchourko, A., Ren, K., Jedicke, O., Melideo, D., Baraldi, D., Slater, S., Duclos, A., Verbecke, F., Molkov, V., 2018. Best practice guidelines in numerical simulations and CFD benchmarking for hydrogen safety applications. Int. J. Hydrogen Energy 44, 9050–9062. https://doi.org/10.1016/j.ijhydene.2018.06.005.

Venetsanos, A.G., Papanikolaou, E., Bartzis, J.G., 2010. The ADREA-HF CFD code for consequence assessment of hydrogen applications. Int. J. Hydrogen Energy 35, 3908–3918. https://doi.org/10.1016/j.ijhydene.2010.01.002.